Mon. Not. R. Astron. Soc. **360,** 839–852 (2005) doi:10.1111/j.1365-2966.2005.09096.x

The 2dF–SDSS LRG and QSO (2SLAQ) Survey: the $z < 2.1$ quasar luminosity function from 5645 quasars to $g = 21.85$

Gordon T. Richards,[1⋆] Scott M. Croom,[2] Scott F. Anderson,[3] Joss Bland-Hawthorn,[2] Brian J. Boyle,[4] Roberto De Propris,[5] Michael J. Drinkwater,[6] Xiaohui Fan,[7] James E. Gunn,[1] Željko Ivezić,[1,3] Sebastian Jester,[8] Jon Loveday,[9] Avery Meiksin,[10] Lance Miller,[11] Adam Myers,[12] Robert C. Nichol,[13] Phil J. Outram,[14] Kevin A. Pimbblet,[6] Isaac G. Roseboom,[6] Nic Ross,[14] Donald P. Schneider,[15] Tom Shanks,[14] Robert G. Sharp,[2] Chris Stoughton,[8] Michael A. Strauss,[1] Alexander S. Szalay,[16] Daniel E. Vanden Berk[15] and Donald G. York[17,18]

[1]*Princeton University Observatory, Peyton Hall, Princeton, NJ 08544, USA*
[2]*Anglo-Australian Observatory, PO Box 296, Epping, NSW 1710, Australia*
[3]*Department of Astronomy, University of Washington, Box 351580, Seattle, WA 98195, USA*
[4]*Australia Telescope National Facility, PO Box 76, Epping, NSW 1710, Australia*
[5]*H. H. Wills Physics Laboratory, University of Bristol, Tyndall Avenue, Bristol BS8 1TL*
[6]*Department of Physics, University of Queensland, Brisbane, QLD 4072, Australia*
[7]*Steward Observatory, University of Arizona, 933 North Cherry Avenue, Tucson, AZ 85721, USA*
[8]*Fermi National Accelerator Laboratory, PO Box 500, Batavia, IL 60510, USA*
[9]*Astronomy Centre, University of Sussex, Falmer, Brighton BN1 9QJ*
[10]*Institute for Astronomy, Royal Observatory, University of Edinburgh, Blackford Hill, Edinburgh EH9 3HJ*
[11]*Department of Physics, Oxford University, 1 Keble Road, Oxford OX1 3RH*
[12]*Department of Astronomy, University of Illinois at Urbana–Champaign, 1002 West Green Street, Urbana, IL 61801-3080, USA*
[13]*Institute of Cosmology and Gravitation, Mercantile House, Hampshire Terrace, University of Portsmouth, Portsmouth PO1 2EG*
[14]*Department of Physics, University of Durham, South Road, Durham DH1 3LE*
[15]*Department of Astronomy and Astrophysics, The Pennsylvania State University, 525 Davey Laboratory, University Park, PA 16802, USA*
[16]*Department of Physics and Astronomy, The Johns Hopkins University, 3400 North Charles Street, Baltimore, MD 21218-2686, USA*
[17]*Department of Astronomy and Astrophysics, The University of Chicago, 5640 South Ellis Avenue, Chicago, IL 60637, USA*
[18]*Enrico Fermi Institute, The University of Chicago, 5640 South Ellis Avenue, Chicago, IL 60637, USA*

Accepted 2005 April 8. Received 2005 March 24; in original form 2005 February 9

ABSTRACT

We have used the Two-Degree Field (2dF) instrument on the Anglo-Australian Telescope (AAT) to obtain redshifts of a sample of $z < 3$ and $18.0 < g < 21.85$ quasars selected from Sloan Digital Sky Survey (SDSS) imaging. These data are part of a larger joint programme between the SDSS and 2dF communities to obtain spectra of faint quasars and luminous red galaxies, namely the 2dF–SDSS LRG and QSO (2SLAQ) Survey. We describe the quasar selection algorithm and present the resulting number counts and luminosity function of 5645 quasars in 105.7 deg^2. The bright-end number counts and luminosity functions agree well with determinations from the 2dF QSO Redshift Survey (2QZ) data to $g \sim 20.2$. However, at the faint end, the 2SLAQ number counts and luminosity functions are steeper (i.e. require more faint quasars) than the final 2QZ results from Croom et al., but are consistent with the preliminary 2QZ results from Boyle et al. Using the functional form adopted for the 2QZ analysis (a double power law with pure luminosity evolution characterized by a second-order polynomial in redshift), we find a faint-end slope of $\beta = -1.78 \pm 0.03$ if we allow all of the parameters to vary, and $\beta = -1.45 \pm 0.03$ if we allow only the faint-end slope and normalization to vary (holding all other parameters equal to the final 2QZ values). Over the magnitude range covered by the 2SLAQ survey, our maximum-likelihood fit to the data yields 32 per cent more quasars than the final 2QZ parametrization, but is not inconsistent with other $g > 21$ deep surveys for

⋆E-mail: gtr@astro.princeton.edu

quasars. The 2SLAQ data exhibit no well-defined 'break' in the number counts or luminosity function, but do clearly flatten with increasing magnitude. Finally, we find that the shape of the quasar luminosity function derived from 2SLAQ is in good agreement with that derived from Type I quasars found in hard X-ray surveys.

Key words: surveys – galaxies: active – quasars: general – galaxies: Seyfert – cosmology: observations.

1 INTRODUCTION

We have merged the high-quality digital imaging of the Sloan Digital Sky Survey (SDSS; York et al. 2000) and the powerful spectroscopic capabilities of the Two-Degree Field (2dF) instrument (Lewis et al. 2002) to conduct a deep wide-field spectroscopic survey for quasars (quasi-stellar objects, QSOs) and luminous red galaxies (LRGs), i.e. the 2dF–SDSS LRG and QSO Survey (hereafter referred to as 2SLAQ). The combination of these facilities allows us to probe substantially deeper than either the SDSS or 2dF surveys can individually. This paper describes the first results of the quasar aspect of the survey; see Cannon et al. (2003), Padmanabhan et al. (2005) and Cannon et al. (in preparation) for a discussion of the LRG component of the survey.

The 2dF QSO Redshift Survey (2QZ; Boyle et al. 2000; Croom et al. 2004) was restricted to $b_J < 20.85$. We use the SDSS imaging data as the input for a new survey, allowing us to probe to $g = 21.85$ with typical photometric errors at the flux limit of only 7 per cent – considerably fainter than either the $i = 19.1$ flux limit of the SDSS Quasar Survey (Richards et al. 2002; Schneider et al. 2003) or the $b_J = 20.85$ flux limits of 2QZ. By allocating 200 fibres per 2dF plate to this new quasar survey (with an additional 200 fibres going to LRGs), and extending the exposure time to 4 h (compared to $\sim$1 h for SDSS and 2QZ), we hope to obtain spectra of 10 000 quasars to $g = 21.85$ in the next few years. This paper reports on the first three semesters of data (with 5645 quasars) and presents the $z < 2.1$ quasar luminosity function (QLF) to fainter luminosities at each redshift than either the SDSS or 2QZ surveys alone.

The first determination of the luminosity function of quasars was by Schmidt (1968). Subsequent pioneering work was carried out by many groups including Schmidt & Green (1983), Koo & Kron (1988), Hewett, Foltz & Chaffee (1993) and especially Boyle and collaborators (e.g. Boyle, Shanks & Peterson 1988), with extensions to high z ($z > 3$) being provided by Warren, Hewett & Osmer (1994), Schmidt, Schneider & Gunn (1995), Kennefick, Djorgovski & de Carvalho (1995) and Fan et al. (2001a). The largest samples analysed to date come from the 2dF QSO Redshift Survey (Boyle et al. 2000; Croom et al. 2004) with 23 338 quasars.

With the exception of variability-selected samples (e.g. Hawkins & Veron 1995), early QLF determinations were generally characterized by a strong, distinct 'break' whose redshift evolution has been the subject of much discussion. However, more recent determinations (e.g. COMBO-17; Wolf et al. 2003), while still exhibiting distinct curvature in a log–log plot, show less of a break at a specific luminosity.

Recently, optical surveys have been supplemented by X-ray surveys (both soft and hard) that, when correcting for selection differences, can largely reproduce the optical Type I QLF (e.g. Ueda et al. 2003; Barger et al. 2005). These X-ray QLFs have also been shown to exhibit a break, but generally at luminosities much fainter than found by optical surveys; this result suggests incompleteness at the faint end of optical surveys.

As we shall see, our data are in good agreement with recent results for faint quasars from both the optical (e.g. Wolf et al. 2003) and X-ray (e.g. Barger et al. 2005). We probe nearly 1 mag deeper than 2QZ, and find that the faint-end slope of the QLF is steeper than that of the most recent 2QZ determination and lacks a strong characteristic break feature, but is still better characterized by a double power law than a single power law.

Section 2 presents a description of the imaging data and the sample selection. In Section 3 we describe the observations and data reduction. Section 4 presents the completeness corrections leading to the QLF presented in Section 5. Finally, Section 6 presents a discussion of the ramifications of our work and summarizes our results. Throughout this paper we use a cosmology with $H_0 = h_{70}$ 70 km s^{-1} Mpc^{-1}, $\Omega_m = 0.3$ and $\Omega_\Lambda = 0.7$ (e.g. Spergel et al. 2003).

2 THE IMAGING DATA AND SAMPLE SELECTION

2.1 The SDSS imaging data

The photometric measurements used as the basis for our catalogue are drawn from SDSS imaging data (DR1 reductions; Stoughton et al. 2002; Abazajian et al. 2003), which will eventually cover roughly 10 000 deg^2 of sky in five photometric passbands (*ugriz*) using a large-format charge-coupled device (CCD) camera (Gunn et al. 1998). The photometric system and its characterization are discussed by Fukugita et al. (1996), Hogg et al. (2001), Smith et al. (2002) and Stoughton et al. (2002); the spectroscopic tiling algorithm is described by Blanton et al. (2003). Except where otherwise stated, all SDSS magnitudes discussed herein are 'asinh' point spread function (PSF) magnitudes (Lupton, Gunn & Szalay 1999) on an AB magnitude system (Oke & Gunn 1983) that have been dereddened for Galactic extinction according to the model of Schlegel, Finkbeiner & Davis (1998). The astrometric accuracy of the SDSS imaging data is better than 100 mas per coordinate rms (Pier et al. 2003). The SDSS Quasar Survey (Richards et al. 2002; Schneider et al. 2003, 2005) extends to $i = 19.1$ for $z < 3$ and to $i = 20.2$ for $z > 3$, whereas our work herein explores the $z < 3$ regime to $g = 21.85$ ($i \sim 21.63$).

2.2 Preliminary sample restrictions

Our quasar candidate sample was drawn from 10 SDSS imaging runs (see Section 2.4) after having first been vetted of objects that have cosmetic defects (e.g. bad columns) that might cause the photometry to be inaccurate. Specifically, we rejected any objects that met the

'fatal' or 'non-fatal' error definitions as described by Richards et al. (2002).

We next imposed limits on the *i*-band PSF magnitude and its estimated 1σ error of $i < 22.0$ and $\sigma_i < 0.2$. Further magnitude cuts are done in the *g* band (to facilitate comparisons with previous 2QZ results in b_J); the *i*-band cuts are primarily to reduce the number of objects that we have to examine initially. We also placed restrictions on the errors in each of the other four bands, specifically, $\sigma_u < 0.4$, $\sigma_g < 0.13$, $\sigma_r < 0.13$ and $\sigma_z < 0.6$. These restrictions are designed to ensure that the errors on the magnitudes are reasonably small (and thus that the resulting colours are accurate), but also are sufficiently relaxed that, when coupled with the magnitude cut in *i* and *g*, objects with quasar-like continua are not rejected. This tolerance is necessary since, as we go fainter, restrictions on magnitude errors are effectively cuts in magnitude and any two such restrictions are effectively colour cuts. Note that this selection of error constraints effectively limits the redshift to less than 3, as the Lyα forest suppresses the *u* flux at higher redshifts.

2.3 Colour cuts

Based on spectroscopic identifications from SDSS and 2QZ of this initial set of objects, we implement additional colour cuts that are designed to select faint quasars efficiently while maintaining a high degree of completeness to known ultraviolet-excess broad-line quasars. An analysis of the completeness of the selection algorithm is given as a function of redshift and magnitude in Section 4.2.

We first impose colour restrictions that are designed to reject hot white dwarfs. These cuts are made regardless of magnitude. Specifically, we rejected objects that satisfy the condition: A&& ((B&&C&&D)||E), where the letters refer to the cuts:

$$\begin{array}{lrcccl} \text{(A)} & -1.0 & < & u-g & < & 0.8, \\ \text{(B)} & -0.8 & < & g-r & < & 0.0, \\ \text{(C)} & -0.6 & < & r-i & < & -0.1, \\ \text{(D)} & -1.0 & < & i-z & < & -0.1, \\ \text{(E)} & -1.5 & < & g-i & < & -0.3. \end{array} \quad (1)$$

This is similar to the white dwarf cut applied by Richards et al. (2002, equation 2) except for the added cut with respect to the $g-i$ colour.

As the targets become fainter and the magnitude errors increase, we find that maximizing our completeness and efficiency is best served by separate handling of bright and faint objects. The bright sample is restricted to $18.0 < g < 21.15$ and is designed to allow for overlap with previous SDSS and 2dF spectroscopic observations. The faint sample has $21.15 \leqslant g < 21.85$ and probes roughly 1 mag deeper than 2QZ. These cuts are made in *g* rather than *i* (as the SDSS quasar survey does) since we are concentrating on ultraviolet-excess (UVX) quasars and would like to facilitate comparison with the results from the b_J-based 2QZ. The combination of the $g < 21.85$ and $i < 22.0$ cuts will exclude objects bluer than $\alpha_\nu = +0.3$ ($f_\nu \propto \nu^\alpha$); however, objects this blue are exceedingly rare ($>3\sigma$ deviations).

Further cuts are made as a function of colour and morphology in each of the bright/faint samples. In general, we would prefer not to make a cut on morphology since we do not want to exclude low-*z* quasars and because our selection extends beyond the magnitude limits at which the SDSS's star–galaxy separation breaks down. However, Scranton et al. (2002) have developed a Bayesian star–galaxy classifier that is robust to $r \sim 22$. As a result, in addition to straight colour cuts, we also apply some colour restrictions on objects with high *r*-band galaxy probability (referred to below as 'galprob') according to Scranton et al. (2002) in an attempt to remove contamination from narrow emission-line galaxies (NELGs; i.e. blue star-forming galaxies) from our target list.

Bright sample objects are those with $18.0 < g < 21.15$ and that meet the following conditions:

$$\begin{array}{llcccccccl} \text{(A)} & u-g & < & 0.8 & \&\& & g-r & < & 0.6 & \&\& \\ & r-i & < & 0.6, & & & & & & \\ \text{(B)} & u-g & > & 0.6 & \&\& & g-i & > & 0.2, & \\ \text{(C)} & u-g & > & 0.45 & \&\& & g-i & > & 0.35, & \\ \text{(D)} & \text{galprob} & > & 0.99 & \&\& & u-g & > & 0.2 & \&\& \\ & g-r & > & 0.25 & \&\& & r-i & < & 0.3, & \\ \text{(E)} & \text{galprob} & > & 0.99 & \&\& & u-g & > & 0.45, & \end{array} \quad (2)$$

in the combination A&&!B&&!C&&!D&&!E, where cut A selects UVX objects, cuts B and C eliminate faint F stars whose metallicity and errors push them blueward into the quasar regime, and cuts D and E remove NELGs that appear extended in the *r* band. Among the bright sample objects, those with $g > 20.5$ were given priority in terms of fibre assignment.

Faint sample objects are those with $21.15 \leqslant g < 21.85$ and that meet the following conditions:

$$\begin{array}{llcccccccl} \text{(A)} & u-g & < & 0.8 & \&\& & g-r & < & 0.5 & \&\& \\ & r-i & < & 0.6, & & & & & & \\ \text{(B)} & u-g & > & 0.5 & \&\& & g-i & > & 0.15, & \\ \text{(C)} & u-g & > & 0.4 & \&\& & g-i & > & 0.3, & \\ \text{(D)} & u-g & > & 0.2 & \&\& & g-i & > & 0.45, & \\ \text{(E)} & \text{galprob} & > & 0.99 & \&\& & g-r & > & 0.3, & \end{array} \quad (3)$$

in the combination A&&!B&&!C&&!D&&!E, where cut A selects UVX objects, cuts B, C and D eliminate faint F stars whose metallicity and errors push them blueward into the quasar regime, and cut E removes NELGs. These faint cuts are more restrictive than the bright cuts to avoid significant contamination from main-sequence stars that will enter the sample as a result of larger errors at fainter magnitudes.

Fig. 1 shows the $u-g$ versus $g-i$ colour distribution of objects satisfying these criteria for which we obtained new spectra. Objects confirmed to be quasars are shown in black, while those that are not quasars (mostly stars and NELGs) are shown in red. The locus of $z < 3$ quasars from SDSS-DR1 (Schneider et al. 2003) is given by grey contours and points. Solid blue, dashed blue and dotted cyan lines show the faint sample colour cuts, the bright sample colour cuts and the white dwarf cut, respectively.

2.4 Sky location of imaging data

2.4.1 2003A and 2004A

For the first semester both of 2003 and 2004, we used the SDSS imaging data (rerun 20; Stoughton et al. 2002; Abazajian et al. 2003) in the SDSS northern equatorial scan (stripe 10) from runs 752, 756, 1239 and 2141; see York et al. (2000) and Stoughton et al. (2002) for the definition of the relevant SDSS technical terms. Run 756 was used for the northern part of the stripe, while a combination of the other three runs was used for the southern part of the stripe in an attempt to use the best-quality data (typically that with the best seeing). The area of sky sampled was further limited to regions where the SDSS image quality was deemed to be good enough to use for targeting faint objects for spectroscopy, specifically seeing $\leqslant$1.8 arcsec and *r*-band Galactic extinction $\leqslant$0.2 (Schlegel et al. 1998). We also excluded any objects from SDSS camera column 6, since 2dF cannot cover the full 2°.5 wide SDSS stripe and column 6 has the lowest-quality data of all the columns as a result

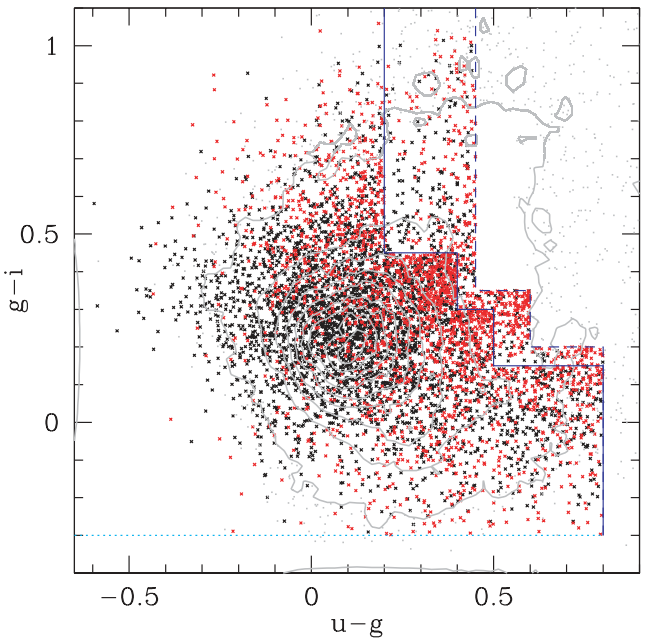

Figure 1. Colours of spectroscopically identified 2SLAQ targets. Confirmed quasars are shown in black, and non-quasars in red. For reference, the colour distribution of $z < 3$ SDSS-DR1 quasars (Schneider et al. 2003) are shown as faint grey contours/points. The dashed and solid dark blue lines show the $u - g$ and $g - i$ colour cuts for the bright and faint samples, respectively. The dotted cyan line shows the boundary of the $g - i$ cut used to reject white dwarfs.

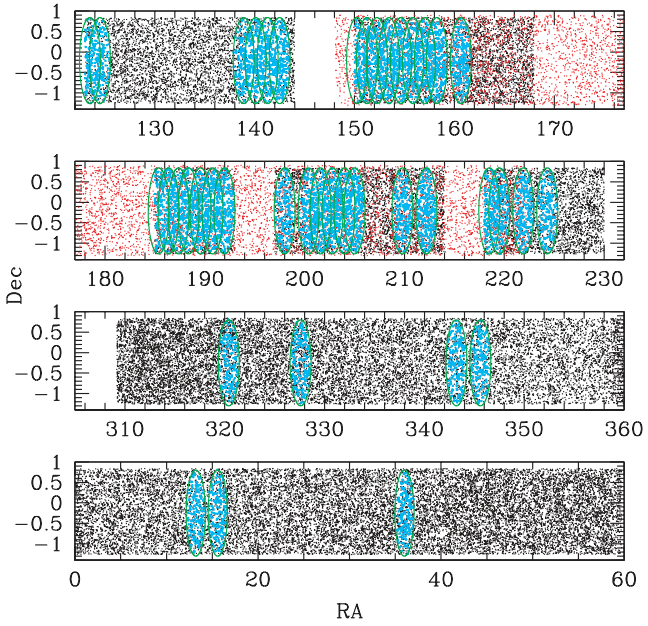

Figure 2. RA and Dec. distribution of 2dF targets selected from SDSS imaging data (black) and previous 2dF observations (red). 2SLAQ observations are given by cyan points within 41 plates (green circles). The top two panels are semester A targets; the bottom two panels are semester B targets. Note the distortion of the coordinate system; the spectroscopic plates are actually circular.

of (relatively) poorer image quality at the edge of the camera in these early SDSS data. The final RA ranges were $123^\circ < \alpha_{J2000} < 144^\circ$, $150^\circ < \alpha_{J2000} < 168^\circ$, $185^\circ < \alpha_{J2000} < 193^\circ$, $197^\circ < \alpha_{J2000} < 214^\circ$ and $218^\circ < \alpha_{J2000} < 230^\circ$. Whenever possible, we tried to overlap areas with existing 2QZ spectroscopy to limit the number of objects with $b_J < 20.85$ that needed spectroscopic confirmation. SDSS spectroscopy limits the need for new $i < 19.1$ spectra. The two top panels of Fig. 2 illustrate the area covered by our semester A targets ($-1\overset{\circ}{.}259 \leqslant \delta_{J2000} \leqslant 0\overset{\circ}{.}840$).

2.4.2 2003B

For the second semester, our samples were limited to the following combination of data (run, rerun, strip, α_{J2000} range):

(2659, 40, 82N, $309\overset{\circ}{.}0 < \alpha_{J2000} < 320\overset{\circ}{.}34$),
(2662, 40, 82N, $320\overset{\circ}{.}34 < \alpha_{J2000} < 15\overset{\circ}{.}08$),
(2738, 40, 82N, $15\overset{\circ}{.}08 < \alpha_{J2000} < 59\overset{\circ}{.}70$),
(2583, 40, 82S, $309\overset{\circ}{.}20 < \alpha_{J2000} < 341\overset{\circ}{.}08$),
(3388, 40, 82S, $341\overset{\circ}{.}08 < \alpha_{J2000} < 345\overset{\circ}{.}44$),
(3325, 41, 82S, $345\overset{\circ}{.}44 < \alpha_{J2000} < 59\overset{\circ}{.}70$).

These reruns (40 and 41) represent post-DR1 data processing, which includes a newer version of the photometric pipeline and improved photometric calibration. Again, camera column 6 was excluded and these are all equatorial scans. Note that there are no 2QZ observations in this range. The two bottom panels of Fig. 2 illustrate the area covered by our semester B targets.

2.4.3 Sky area

The area of sky covered by our catalogue of targets for 2003/4A was 159.4 deg^2 with 20 228 targets, and for 2003B it was 230.2 deg^2 with 33 160 total targets. Thus we have a total area of 389.6 deg^2 and 53 388 targets. Of this area, this paper concentrates on only those regions where we have obtained new spectra (see Fig. 2). In semester 2003/4A, 34 plates were observed, covering an area of 80.82 deg^2 – as determined by the fraction of targets within the plate areas (11 075 of 53 388). In the second semester, seven plates were observed, covering an area of 24.9 deg^2 (3407 of 53 388 targets within the new plate areas). Note that the plates overlapped in 2003/4A, but not in 2003B. The theoretical area for 2003B given a plate radius of $1\overset{\circ}{.}05$ is 24.3 deg^2, which compared to the area estimated by fraction of targets (24.9 deg^2) suggests that our estimate of the area has a roughly 2.5 per cent error. Thus the area covered by new plate observations is 105.7 ± 2.6 deg^2. Within these plate centres there are 14 482 targets, of which 9120 have spectroscopic identifications, and among those are 5645 quasars.

3 SPECTROSCOPIC OBSERVATIONS

3.1 The 2dF facility

The Two-Degree Field (2dF; Lewis et al. 2002) facility at the Anglo-Australian Telescope (AAT) is a fibre-fed multi-object spectrograph and robotic fibre positioner. The fibres are 140 μm in diameter, which is roughly 2.16 arcsec at the centre of the plate and 1.99 arcsec at the edges. Two independent spectrographs use Tektronix 1024 × 1024 CCDs with a range of diffraction gratings offering resolutions between 10 and 2.2 Å over the optical wavelength range. During standard operation, 400 fibres are available for simultaneous observation (200 per spectrograph) over a 2° diameter field of view. The system is equipped with an atmospheric dispersion compensator, which enables 2dF observations to be taken over a wide wavelength range, by ensuring that all wavelengths from the ultraviolet to near-infrared enter the fibres. However, differential

spatial atmospheric refraction distorts the field geometry and limits observations of equatorial fields to ± 1 h on either side of transit.

3.2 2dF field configurations

The 2SLAQ survey regions are centred close to the equator and are 2° wide in declination. To achieve optimal sky coverage while still retaining a largely contiguous area, the 2dF field centres are placed along the central declination of the two strips; $\delta_{J2000} = -00^\circ 12' 35''$ for the North Galactic Pole (NGP) strip and $\delta_{J2000} = -00^\circ 15' 00''$ for the South Galactic Pole strip; see Section 2.4. Each field centre is separated by $1^\circ\!.2$, although some early observations of the NGP at the start of 2003 had field spacings of 1°.

The target list generated from the process described in Section 2 is then merged with a target list of LRGs selected from the same photometric data set (Cannon et al., in preparation). The subsamples within this combined data set are assigned different priorities, which determine the likelihood of a fibre being assigned to them in the 2dF configuration process. The priority values given to each sample are listed in Table 1, where 9 is the highest and 1 the lowest priority. All available high-priority targets are allocated before moving to the next priority level. For source densities much greater than 400 per 2dF field, the 2dF configuration algorithm will tend to give a non-uniform distribution of fibres allocated to objects (Cannon et al., in preparation). Therefore, the main samples of each of the LRG and QSO data sets were randomly sampled to a surface density of 200 per 2dF field, and these given priority 8 and 6 for the LRGs and QSOs, respectively. The remaining sources from these main samples were given lower priority (7 and 5, respectively). Other subsamples, such as bright QSOs and high-redshift candidates, were given lower priority.

For the QSO sample we used the low-resolution 300B grating (as used for the 2QZ), but the LRG observations required the use of the higher-resolution 600V grating. Therefore, one of the 2dF spectrographs is configured with a 300B grating (spectrograph 1) while the second (spectrograph 2) is configured with the 600V grating. On each 2dF field plate of 400 fibres, each block of 10 fibres (a retractor block) goes to an alternate spectrograph, so that 200 fibres on each plate are available for the QSOs and 200 for the LRGs. The 2dF fibres are limited to a maximum off-radial angle of 14°, and therefore there are 20 small triangles surrounding the edge of the 2dF fields that are inaccessible to the QSO spectrograph covering a total area of 0.43 deg^2. The angular completeness function defined by this complex field pattern is not relevant to the QLF analysis below, but it is critical to accurate measurements of clustering. Of the 200 fibres available for the QSOs, 20 were allocated to positions known to be blank sky to be used for sky subtraction.

Table 1. 2dF configuration priorities.

Sample	Priority
Guide stars	9
LRG (main), random	8
LRG (main), remainder	7
QSOs ($g > 20.5$), random	6
QSOs ($g > 20.5$), remainder	5
LRG (extras) + high-z QSOs	4
QSOs ($g < 20.5$)	3
Previously observed	1

3.3 2dF observations and data processing

Observations started in 2003 March. Each 2dF field was observed for a minimum of 4 h (more if weather was poor). These 4 h were split over two nights to minimize the effects of changing atmospheric refraction. The 300B grating used gives a dispersion of 4.3 Å pixel^{-1} and an instrumental resolution of 9 Å. The spectra cover the range 3700–7900 Å. The data were reduced in real time using the standard 2dFDR pipeline (Bailey et al. 2003). The exposure times increased if the conditions meant that a predefined completeness limit (80 per cent) was not met. Any source that has a high signal-to-noise ratio (S/N) spectrum and a high-confidence identification after the first night of observation has its fibre assigned to previously unallocated sources for future observations of the field.

The identification of QSOs and measurement of redshifts were done using the AUTOZ code that was developed for the 2QZ (for details, see Croom et al. 2001, section 3.1; Croom et al. 2004, section 2.3.1). All spectra are then checked by eye to confirm the identifications. Since spectroscopic processing is the same as that used for 2QZ spectra [e.g. quasars must have broad ($>1000\,\mathrm{km\,s^{-1}}$) emission lines], we treat 2SLAQ-selected objects with 2QZ spectra as if they were observed as part of the 2SLAQ programme.

4 COMPLETENESS CORRECTIONS

In this section we explore and quantify the various effects that will bias the quasar number counts and luminosity function. In particular, we address the photometric, coverage, spectroscopic and cosmetic defect incompleteness of our sample. In addition, we investigate the difference between g and b_J magnitudes, Eddington bias, morphology bias and the effects of variability.

4.1 Coverage and spectroscopic completeness

We have not obtained spectra of all our quasar candidates in the 105.7 deg^2 analysed in this paper. Thus we must compute the 'coverage' completeness of our sample, which multiplied by the area yields the effective area of the survey. Since we are combining data from three distinct surveys (SDSS, 2QZ and 2SLAQ) in order to increase our dynamic range, it is necessary to compute this correction as a function of magnitude. The coverage completeness is computed under the assumption that the fraction of objects that remain unobserved (at a given magnitude) will be quasars at the same rate as those that are observed. This assumption is reasonable given that the objects observed are chosen at random. Fig. 3 shows the coverage completeness (solid line) that we compute as a function of magnitude.

In addition to the coverage completeness, we must correct for those cases in which our spectroscopy does not yield an unambiguous identification. Assuming that the fraction of unidentified objects will be quasars at the same rate as those among identified objects (as a function of magnitude), we derive a spectroscopic incompleteness as shown by the dashed line in Fig. 3. This assumption arguably may tend to overestimate the number of unidentified quasars since the spectroscopic completeness may additionally be a function of redshift (because of emission-line effects, which generally facilitate quasar identification) and since *any* completeness determination is certainly a lower limit. However, our spectroscopic completeness is generally high (70 per cent at the faint limit, 90 per cent brighter); thus any second-order corrections will have a minimal impact. Furthermore, comparison with supplementary identifications based solely on photometry and photometric

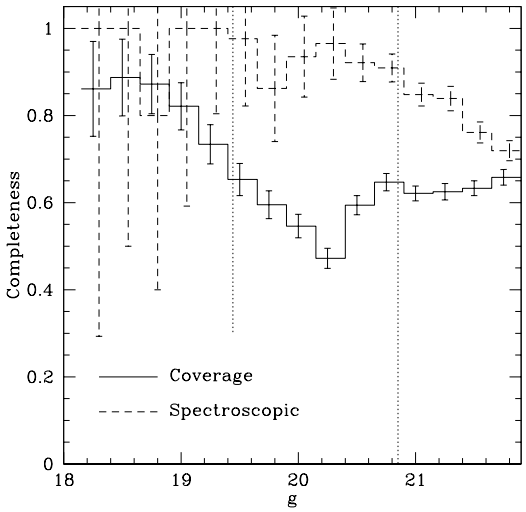

Figure 3. Spectroscopic (dashed line) and coverage (solid line) completeness fractions as a function of magnitude in 0.25 mag bins. These corrections were applied [in conjunction with the photometric completeness correction (Fig. 4)] to determine the corrected number counts. The dotted vertical lines show the boundaries of the SDSS ($i = 19.1$, $g \sim 19.32$) and 2QZ surveys ($b_J \sim g = 20.85$). The discontinuity in coverage completeness at $g \sim 20.5$ is caused by a prioritization of targets fainter than this limit; see Table 1.

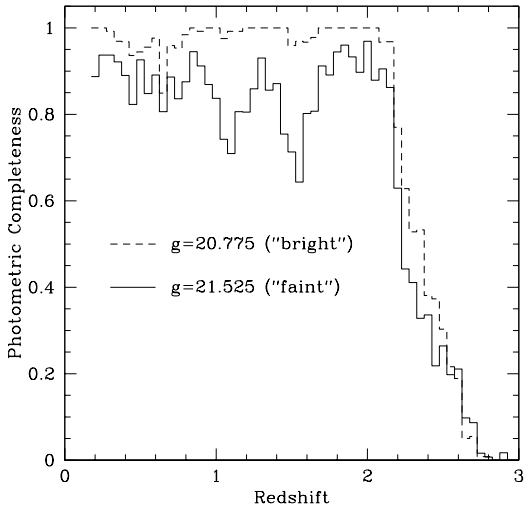

Figure 4. Completeness as a function of redshift and g magnitude based on simulated quasars. Representative magnitude ranges are shown for 'bright' and 'faint' samples with redshift intervals of 0.05.

redshifts (Section 5) suggests that this assumption is reasonable. In practice, we have treated the spectroscopic completeness as if the unidentified objects simply had not been observed, which facilitates the application of these corrections to our model of the luminosity function.

4.2 Photometric completeness

The incompleteness of our sample due to colour cuts is a strong function of both redshift and magnitude since the colours of quasars change significantly with redshift and fainter quasars have larger errors. We quantify this incompleteness by running our selection algorithm on a sample of simulated quasars that were designed to test the SDSS's quasar target selection algorithm; see Fan (1999) and Richards et al. (in preparation). The primary independent variable in the simulations is the spectral index distribution, which is given by a Gaussian distribution with $\alpha_\nu = -0.5 \pm 0.3$ ($f_\nu \propto \nu^{\alpha_\nu}$), which is in good agreement with the composite SDSS quasar spectrum given by Vanden Berk et al. (2001). Blueward of the Lyα emission line we instead use a spectral index of $\alpha_\nu = -1.5 \pm 0.17$, consistent with Telfer et al. (2002); this spectral index is taken to be uncorrelated with the optical/ultraviolet spectral index. Only the spectral index, the Lyα equivalent width and the Lyα forest strength vary; all other emission lines are fixed relative to Lyα.

Fig. 4 shows the selection completeness to these simulated quasars as a function of redshift and g magnitude. Two representative ranges are shown, with bins 0.25 mag wide centred on $g = 20.775$ and 21.525. The $g = 20.775$ completeness curve (dashed line) is representative of the 'bright' sample, whereas the $g = 21.525$ curve (solid line) is representative of the 'faint' sample (except for the faintest bin, since it extends to $g = 21.9$ and the sample only goes to $g = 21.85$). Incomplete redshift regions occur when photometric errors are large and/or emission/absorption lines bring the colours of the quasars near/across the colour cuts (e.g. Richards et al. 2001).

4.3 Correction for cosmetic defects

Certain cosmetic defects within the imaging data cause quasars to be missed from our sample. Thus, we need to make a correction for cosmetic defects in the SDSS data, specifically for those objects that fail the fatal/non-fatal error tests (Richards et al. 2002). One way to quantify this is to assume that any cosmetic defects that prevent the selection of a particular quasar in the SDSS imaging are unlikely to have been present in the 2QZ imaging inputs. With the exception of blended objects, this assumption should be roughly true. Thus we match the NGP sample of quasars from the 2QZ to our initial catalogue of semester A targets (with only the fatal and non-fatal errors, $i < 22$ and $\sigma_i < 0.2$ cuts applied). Since the 2QZ only went to $b_J = 20.85$, the i magnitude cut should not cause us to lose many quasars; however, the fatal and non-fatal error cuts (i.e. cosmetic defects) *will* cause quasars to be lost. The fraction of 2dF quasars that are not among our initial SDSS-imaging-selected sample gives us an estimate of the fraction of quasars that are missed as a result of cosmetic defects. We find that this fraction is ∼5 per cent. A similar fraction is derived by Vanden Berk et al. (2005) based on an empirical analysis of the point-source completeness of the SDSS quasar catalogue. We apply this correction independently of magnitude[1] and redshift in addition to the coverage, spectroscopic and photometric completeness corrections described above. Losses due to blending of sources will increase this completeness correction; for our purposes such losses are assumed to be smaller than the other corrections that we apply.

4.4 Eddington bias

Eddington bias is the distortion of the object number counts as a function of magnitude that occurs when photometric uncertainty causes errors in distributing sources into their proper magnitude bins. The relationship between the observed and actual differential

[1] However, note that Vanden Berk et al. (2005) find that this completeness is a function of magnitude, but the completeness has not been determined at the faint limits to which we are probing, so we assume a uniform value.

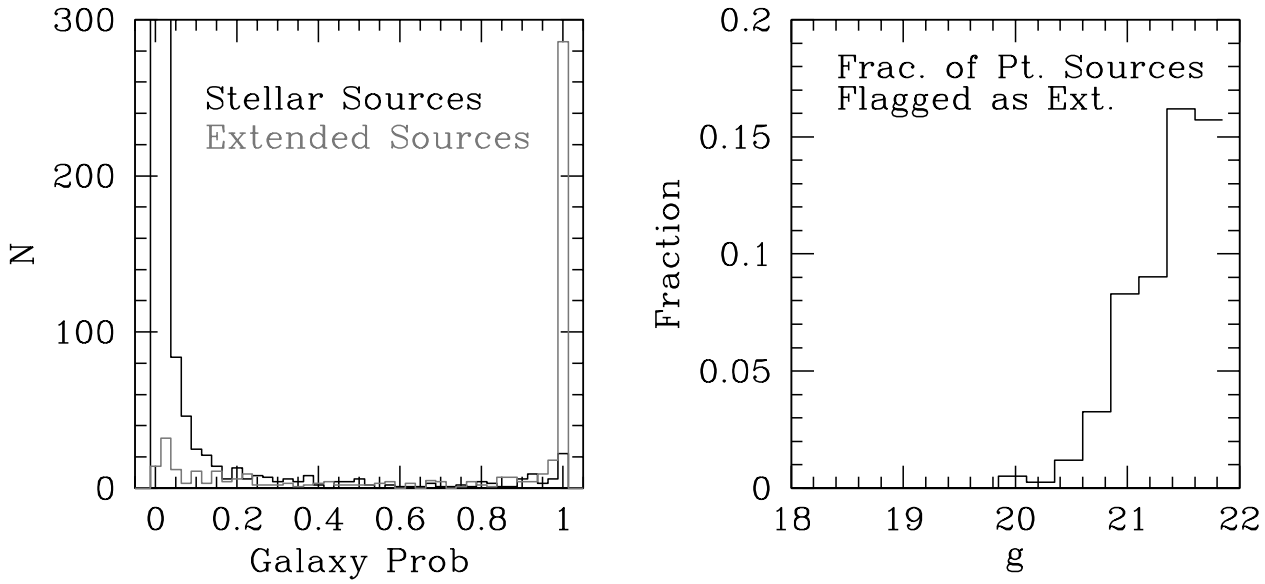

Figure 5. Left: number of spectroscopically confirmed quasars classified by PHOTO as stellar (black) and extended (grey) as a function of Bayesian galaxy probability (Scranton et al. 2002). Right: fraction of point-like quasars (as determined by the Bayesian analysis) that are misclassified by PHOTO as extended – as a function of magnitude.

number counts, $A(m)$, is given by Peterson (1997):

$$A(m) \approx A_{\rm obs}(m)\left[1 - \tfrac{1}{2}(\sigma\kappa/\log {\rm e})^2\right], \quad (4)$$

where σ is the Gaussian error in the magnitude, κ is defined by the integrated number counts relation $N(m) \propto C\ 10^{\kappa m}$, and $\log A(m) = C + \kappa m$. If the product of the slope and the error ($\sigma\kappa$) increases with magnitude, then the observed slope is steeper than the intrinsic slope; for decreasing $\sigma\kappa$, the observed slope is flatter than the intrinsic slope. For our sample, the correction term in brackets above is $\geqslant$0.98 for all magnitude bins; thus we have applied no correction for Eddington bias.

4.5 Morphology bias

Our sample includes objects that the SDSS photometric pipeline (PHOTO; Lupton et al. 2001) classifies as extended. The rationale for this decision is summarized in Fig. 5, which shows that, at the faintest limits of our survey, a significant fraction of point sources are misclassified by the photometric pipeline as extended [assuming that the Bayesian analysis of Scranton et al. (2002) represents ground truth]. The right-hand panel shows that this is a function of magnitude. The left-hand panel shows the Bayesian galaxy probability distribution for both point-like (stellar) and extended quasars as classified by PHOTO.

The inclusion of extended sources can lead to a bias. Specifically, since many of the semester A targets have been observed as part of the 2QZ and since the 2QZ did not target extended sources, our new observations will be preferentially biased towards extended sources. Thus our corrections from the number of objects observed to the number of objects targeted may be skewed since it assumes that new observations will yield quasars at the same rate as old observations. However, we find that, although the contamination among extended sources is larger than for point sources, the *shape* of the corrections as a function of magnitude is not significantly different and thus our analysis of the shape of the QLF should not be adversely affected.

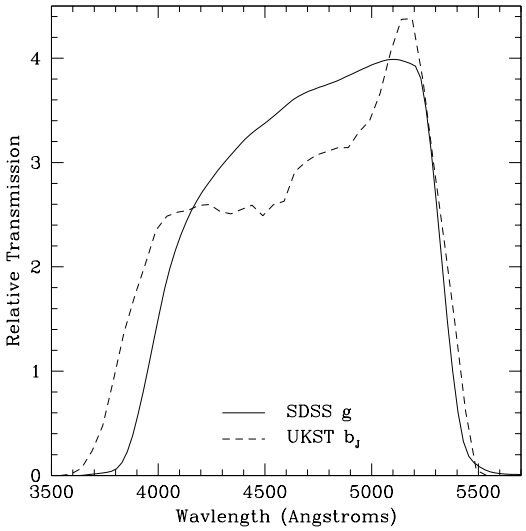

Figure 6. UKST $b_{\rm J}$ (Hewett, private communication) and SDSS g transmission curves for airmass 1 and normalized such that $\int S_\lambda\, {\rm d}\lambda/\lambda = 1$. Both curves are given in terms of detector quantum efficiency, which means that the g curve is shown as published, but the $b_{\rm J}$ curve has been multiplied by wavelength.

4.6 g versus $b_{\rm J}$

To compare our 2SLAQ results properly with those of the 2QZ, we determine the relationship between the SDSS g band and the $b_{\rm J}$ band used by 2dF. Fig. 6 shows the two transmission curves, which are quite similar. The $b_{\rm J}$ curve was kindly provided by Paul Hewett (private communication). The g curve is as taken from the SDSS website[2] – except that it has been converted from airmass 1.3 to airmass 1.0 (to match the $b_{\rm J}$ curve). In Fig. 7, we plot the $g - b_{\rm J}$ magnitude difference versus $b_{\rm J}$ for all of the 2QZ quasars in our

[2] http://www.sdss.org/dr3/instruments/imager/filters/g.dat

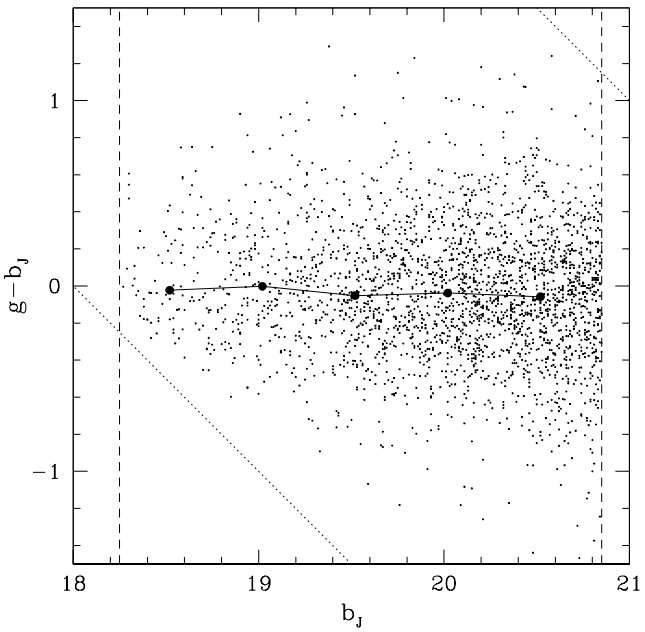

Figure 7. The $g - b_J$ magnitude differences versus b_J, where g is from the SDSS and b_J is from the 2QZ. The dotted lines show the g magnitude limits of the 2SLAQ sample. The dashed lines show the b_J magnitude limits of the 2QZ survey. The points connected by a solid line give the median $g - b_J$ as a function of b_J in 0.5 mag bins. The median over all b_J is $\langle g - b_J \rangle = -0.045$. Neither g nor b_J are extinction-corrected in this plot.

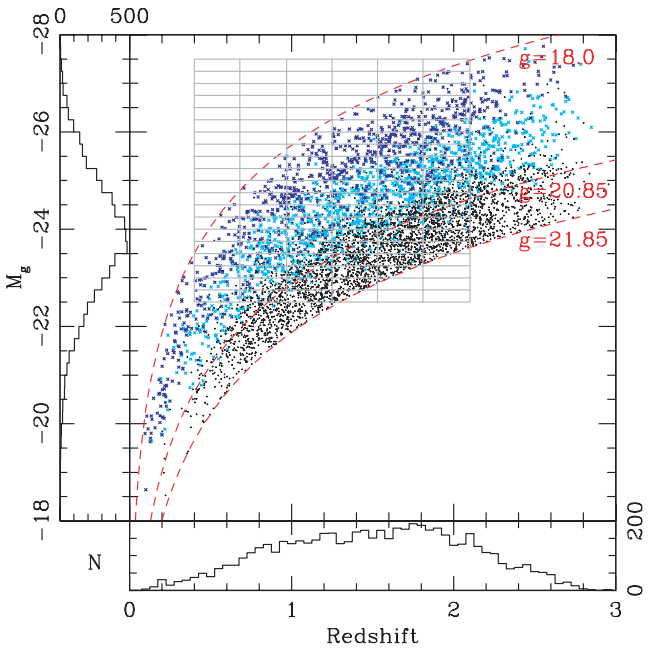

Figure 8. Absolute g magnitude versus redshift for all confirmed quasars in our sample. Blue crosses are SDSS quasars, cyan crosses are 2QZ quasars, and black dots represent quasars confirmed by 2SLAQ. The bottom and side histograms show the 1D distributions of M_g and redshift. The dashed red lines show the bright and faint magnitude limits of this survey ($g = 18.0$ and $g = 21.85$) and the approximate limit of the 2QZ survey in g ($b_J = 20.85$). The grid of grey lines outlines the bins used for determining the quasar luminosity function.

sample. This plot shows that, even considering the scatter in $g - b_J$, the g-band magnitude limits of our current sample completely encompass the 2QZ quasars.

To convert b_J to g we simply compute the median $g - b_J$ difference, which is shown as a function of b_J by points connected by solid lines in Fig. 7. The median for the whole sample is $\langle g - b_J \rangle = -0.045$, with no significant dependence on b_J. Given the empirical similarity of the g and b_J magnitudes, and that the error in the computed median is of the order of the median itself, we have simply taken b_J as an exact surrogate for g in our comparison of the number counts and luminosity functions.

Much of the scatter between b_J and g is caused by variability in the $\geqslant$20 yr between the epochs when the b_J and g data were taken – in contrast with the simultaneity of the SDSS five-band imaging data. The scatter in $g - b_J$ is σ_{g-b_J}=0.25 at $b_J = 18.475$ and σ_{g-b_J}= 0.38 at $b_J = 20.725$. At least 0.15 mag of this error is due to photometric error in b_J (Croom et al. 2004, fig. 9); roughly 0.02 and 0.035 is due to photometric error in g. Thus, most of the scatter (roughly $\sigma \sim 0.2$) is caused by variability. Variability adds uncertainty to the magnitude distribution in the same manner as photometric errors and thus can modify the number counts through Eddington bias. Proper treatment of variability in light of quasar number counts is complicated, ideally using long-term averages of the quasars under consideration. However, we can estimate the effect that variability has on the slope of the number counts. If the variability amplitude is constant with magnitude, then variability will cause a slight flattening of the observed distribution because the number counts will be steeper at the bright end than at the faint end. For $\sigma_{\rm var} = 0.2$, at $g \sim 18.5$ the number counts will be overestimated by $\sim$8 per cent, and at $g \sim 20.7$ they will be overestimated by $\sim$1 per cent, which produces a negligible ($\sim$2 per cent) change in slope over this range.

5 NUMBER COUNTS AND LUMINOSITY FUNCTION

5.1 Redshift and absolute magnitude distributions

Having discussed the various completeness corrections, we can now determine the number counts and luminosity function of our sample. Fig. 8 shows the M_g versus redshift distribution of spectroscopically confirmed 2SLAQ, 2QZ and SDSS quasars in our sample – within the boundaries of new plate observations (105.7 deg^2). The absolute g magnitude, M_g, is computed using luminosity distances in the cosmology given in Section 1 according to the prescription of Hogg (1999) and with the (albeit poor, but commonly used) assumption of a universal power-law continuum of $\alpha_\nu = -0.5$ ($f_\nu \propto \nu^\alpha$).[3] Black, cyan and blue points represent new 2SLAQ quasars, previously confirmed 2QZ quasars and previously confirmed SDSS quasars, respectively. Dashed red lines at $g = 18.0$ and 21.85 demarcate the g-magnitude boundaries of our sample. In addition, we show the $g \sim b_J = 20.85$ limit of the 2QZ survey. The histograms to the left and bottom of the figure show the one-dimensional distribution of sources in M_g and redshift. We further overlay a grid that highlights the magnitude and redshift bins that were used in the construction of the Croom et al. (2004) QLF and will also be used for determining the binned 2SLAQ QLF.

[3] Ideally we would determine a spectral index for each individual object. However, this requires better spectrophotometry/photometry at the faint end than 2SLAQ provides. Fortunately, the errors induced by assuming a fixed spectral index are mitigated by the $z < 2.1$ nature of our analysis (the errors increase with redshift) and the fact that the majority of quasars have roughly this spectral index.

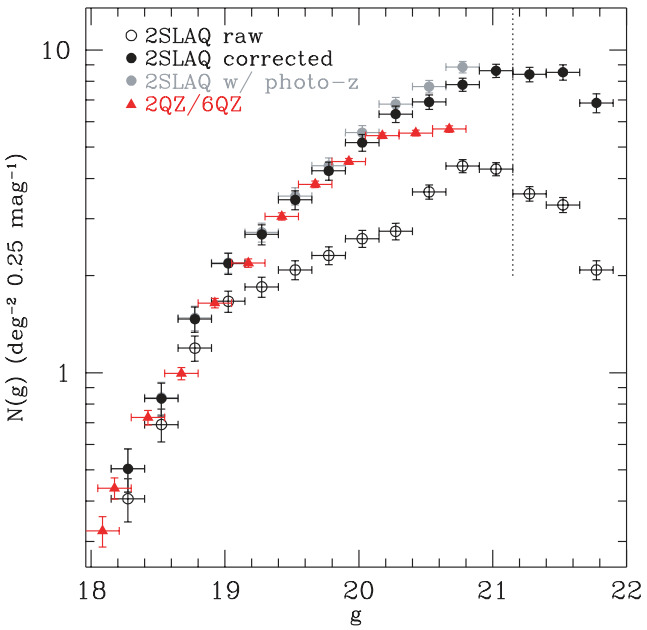

Figure 9. 2SLAQ number counts (black circles) compared to 2QZ number counts (red filled triangles) from Croom et al. (2004). The 2SLAQ number counts are given as both raw (i.e. observed; open circles) and corrected (filled circles) number counts. 2SLAQ number counts are also given (as grey circles) after including photometrically identified quasars (with photometric redshifts) from Richards et al. (2004a). Quasars are restricted to those with $M_g < -22.5$ and $0.4 < z < 2.1$ (3889 quasars) for comparison with the 2QZ number counts. The dotted vertical line marks the dividing line between the 2SLAQ bright and faint samples.

5.2 Number counts

Fig. 9 shows the differential number counts as a function of g magnitude in bins of 0.25 mag, both corrected (solid circles) and uncorrected (open circles) for the various sources of incompleteness (error bars are Poisson). Number counts from 2QZ (Croom et al. 2004) are shown in red for comparison. This diagram only includes quasars with $M_g < -22.5$ and $0.4 < z < 2.1$.

From Fig. 9 we see that to $g \sim 20.2$ the agreement between 2SLAQ and 2QZ is quite good, but there is a discrepancy between the two studies at the faint end: 2SLAQ suggesting a higher density of faint objects than 2QZ. We note that the shape of the distribution is clearly better fitted by a double power law than a single power law (demonstrating the turnover in the distribution towards fainter quasars), but that the change in slope is more subtle than the distinctive 'break' near $g \sim 19.5$ that is sometimes found in such analyses (e.g. Boyle et al. 1987). This behaviour is qualitatively consistent with that found by Wolf et al. (2003) from the COMBO-17 survey and is inconsistent with the single power-law form found in variability-selected samples (e.g. Hawkins & Veron 1995, but see Ivezić et al. 2004).

We have shown (as open circles) the raw number counts to give the reader an idea of the absolute lower limits on the points and the size of the completeness corrections that have been applied. The coverage corrections are straightforward and should be fairly robust (perhaps less so in the three faintest bins due to the more restrictive selection criteria and larger photometric error). In fact, we could have simply corrected the effective area as a function of magnitude and shown the (more complete and much smoother) area-corrected raw counts. However, as we are splicing together three samples (SDSS, 2QZ and 2SLAQ) to provide spectroscopic coverage of our targets, it seems appropriate to disclose fully the magnitude dependence of the coverage completeness within the 105.7 deg^2 area covered by the 2SLAQ plates. As a check on our correction terms, we have also matched our unobserved and unidentified objects to the photometric quasar candidate catalogue of Richards et al. (2004a), in an attempt to 'observe' a larger fraction of our quasar candidates (to $g < 21$). The objects from Richards et al. (2004a) are expected to be 95 per cent accurate (averaged over all magnitudes) with respect to quasar classification, with 90 per cent having photometric redshifts correct to $|\Delta z| \pm 0.3$ for the redshift range considered here (Weinstein et al. 2004). The result of including these photometric identifications is shown by the grey points in Fig. 9, and lends credence to the steeper faint-end number counts relations that we derive solely from our (completeness-corrected) spectroscopic sample. This comparison is meant purely as a sanity check. The differences between the spectroscopic (black circles) and photometric (grey circles) number counts are consistent with the expected decrease in efficiency of the Richards et al. (2004a) photometric catalogue with fainter magnitude, thus supporting the accuracy of our completeness determinations (and our corrected number counts).

We further compare our results to a number of other samples of faint quasars that pre-date the 2QZ sample. This comparison is shown in Fig. 10. Here we have restricted our sample to $0.6 < z < 2.2$ and $M_g < -23$ to best mimic the limits of these previous surveys, which generally excluded extended sources (which typically have $z < 0.6$ or $M_g > -23$). We specifically compare our 2SLAQ results to the samples of Boyle et al. (1988), Koo & Kron (1988), Marano, Zamorani & Zitelli (1988), Boyle et al. (1990), Boyle, Jones & Shanks (1991) and Zitelli et al. (1992), where table 8 in

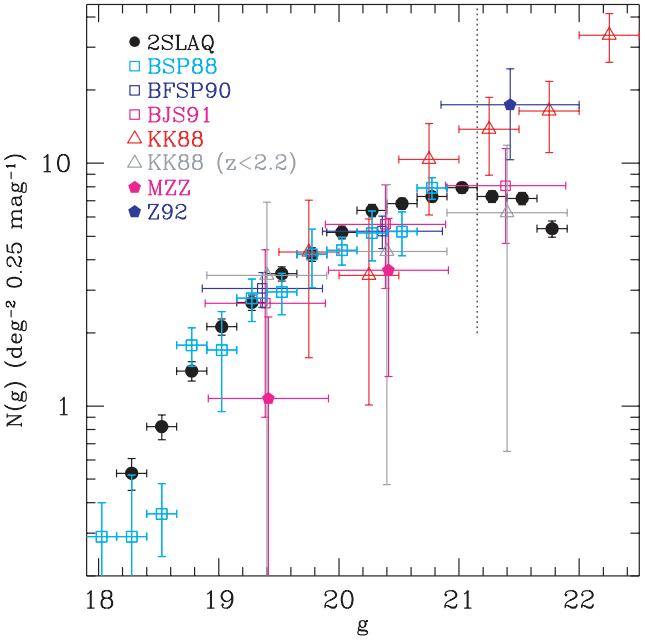

Figure 10. Comparison of 2SLAQ quasar number counts to previous deep samples. 2SLAQ quasars are limited to $M_g < -23$ and $0.6 < z < 2.2$ to mimic the exclusion of extended sources (which mostly have $z < 0.6$ or $M_g > -23$). Open squares indicate points from Boyle and collaborators, specifically Boyle et al. (1988, cyan), Boyle et al. (1990, blue) and Boyle et al. (1991, BJS91, magenta). Open triangles refer to Koo & Kron (1988), where the red triangles are for $0.9 < z < 3.0$ and the grey triangles are for $z < 2.2$ (and $z > 0.9$) as given by table 8 in BJS91. Filled magenta pentagons refer to Marano et al. (1988), as given by table 8 in BJS91. The filled blue pentagon is derived from Zitelli et al. (1992).

Boyle et al. (1991) is the source of the Boyle et al. (1990), Zitelli et al. (1992) and Koo & Kron (1988) ($z < 2.2$) points. The redshift ranges and magnitude calibrations between all of these samples do not match exactly, but they suffice to give the reader an idea of how our results compare with past work. In particular, in comparison with previous work, we note that while the 2SLAQ data show an excess at $20 < g < 20.6$, they generally show a deficit for $g > 20.6$. The one exception is the faintest $z < 2.2$ point from Koo & Kron (1988); however, that sample has a lower redshift limit of $z \sim 0.9$, whereas our sample extends to lower redshift. Overall, to the limit of our bright sample ($g < 21.15$), our agreement with previous work is well within the errors. Fainter than $g = 21.15$, if anything, the 2SLAQ counts are deficient, but are still consistent considering the large coverage and spectroscopic completeness corrections at these limits. Fig. 11 shows the cumulative 2SLAQ and 2QZ/6QZ quasar number counts. At the limit of the 2SLAQ survey, the cumulative counts compare well with the $J = 22$ cumulative counts (86.3 ± 16.5) from Zitelli et al. (1992). The slope of the cumulative counts are given as three-bin averages by the dashed lines and the numbers at the bottom of the plot. The brightest 2SLAQ points are unreliable, as 2SLAQ does not include quasars brighter than $g = 18$. The cumulative 2QZ/6QZ number counts give a better idea of the slope at the bright end. Table 2 shows a comparison of the cumulative number counts predicted by the Boyle et al. (2000), Croom et al. (2004) and 2SLAQ best-fitting maximum-likelihood parametrizations (assuming a double power law and luminosity evolution characterized by a second-order polynomial) for $g > 16.0$ and $0.3 < z < 2.2$.

5.3 Luminosity function

Fig. 12 shows two determinations of luminosity function derived from our sample. We first use the Page & Carrera (2000) implementation of the $1/V$ method (Schmidt 1968; Avni & Bahcall 1980), which is shown by the points with error bars. This implementation corrects for incompleteness at both the bright and faint limits of the survey. These incomplete bins (those not filled in Fig. 8) are shown as open rather than closed points to indicate that they have been corrected for partial coverage of the bin. However, we note that the Page & Carrera (2000) correction for incomplete bins is not fully accurate since the (relatively large) $z - M_g$ bins are not uniformly sampled (see Fig. 8). The redshifts are the same as those in fig. 20 of Croom et al. (2004) for ease of comparison. The size of the redshift bins is $\Delta z = 0.283$, and the $z = 1.39$ data are repeated as grey lines in each panel.

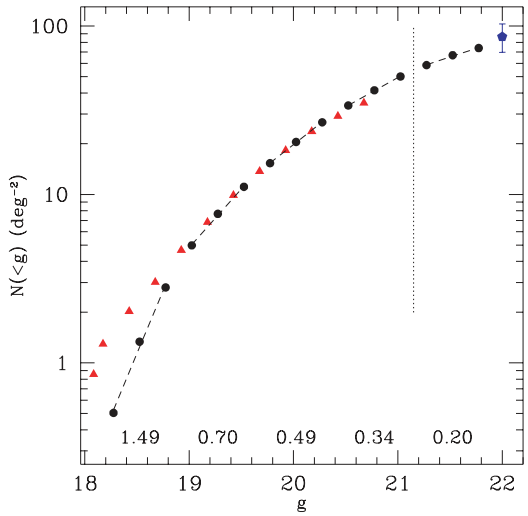

Figure 11. Cumulative 2SLAQ (black circles) and 2QZ (red triangles) as a function of g. The numbers at the bottom indicate the slope of the three-bin least-squares fits shown by the series of dashed lines. Note that the bright limit of the 2SLAQ data is $g = 18$, which causes a deficiency in the cumulative number counts at the bright end; at the faint end this lack of bright quasars makes little difference. While there is no strong characteristic break, the number counts clearly flatten with fainter magnitude. The blue pentagon shows the cumulative J-band number counts from Zitelli et al. (1992).

Table 2. Cumulative number count comparison. The cumulative number counts are shown for the Boyle et al. (2000, B00), Croom et al. (2004, C04) and 2SLAQ maximum-likelihood parametrizations for $16 < g < x$ mag and $0.3 < z < 2.2$ in unit of counts per square degree.

x (mag)	B00	C04	2SLAQ
20.0	15.87	17.50	18.96
20.5	26.99	28.27	31.09
21.0	41.68	40.22	47.79
21.5	59.45	52.01	69.13
22.0	78.88	62.46	93.77

We next give the luminosity function as derived from a maximum-likelihood analysis; these are plotted as dashed/solid lines, the dashed part indicating extrapolation beyond the data used for the fit. The cyan lines show the best-fitting double power-law model (see below) from row 1 in table 6 of Croom et al. (2004), which provide a poor fit at the faint end. The yellow lines show a similar model from row 1 in table 3 of Boyle et al. (2000) (corrected to our cosmology), which has a steeper faint-end slope. Our own fit is shown in red and was derived as described below.

We have assumed a luminosity function in the standard form of a double power law (Peterson 1997; Croom et al. 2004)[4]

$$\Phi(L_g, z) = \frac{\Phi\left(L_g^*\right)/L_g^*}{\left(L_g/L_g^*\right)^{-\alpha} + \left(L_g/L_g^*\right)^{-\beta}} \tag{5}$$

or

$$\Phi(M_g, z) = \frac{\Phi\left(M_g^*\right)}{10^{0.4(\alpha+1)(M_g - M_g^*)} + 10^{0.4(\beta+1)(M_g - M_g^*)}}. \tag{6}$$

We assume that the evolution with redshift is characterized by pure luminosity evolution (individual quasars getting fainter from $z = 2$ to today), with the dependence of the characteristic luminosity described by a second-order polynomial in redshift as in Croom et al. (2004) where

$$M_g^*(z) = M_g^*(0) - 2.5\left(k_1 z + k_2 z^2\right). \tag{7}$$

Note that this form assumes symmetric redshift evolution about the peak. This assumption is appropriate for UVX samples such as this one, but will break down for samples that extend to higher redshifts (e.g. Richards et al., in preparation).

We compute the maximum-likelihood solution via Powell's method (Press et al. 1992) using the form given by Fan et al. (2001a). We first attempt to determine the best-fitting parameters by allowing all of the parameters to vary. The resulting parameters are given

[4] We remind the reader of the well-known sign error in Boyle et al. (2000) whereby (in the convention used herein) the first equation in their section 3.2.2 should have negative signs on α and β and the entries for α and β in tables 2 and 3 should be multiplied by -1. In addition, equation (10) in Croom et al. (2004) and the equivalent equation in Section 3.2.2 of Boyle et al. are missing a $1/L^*$ factor in the numerator.

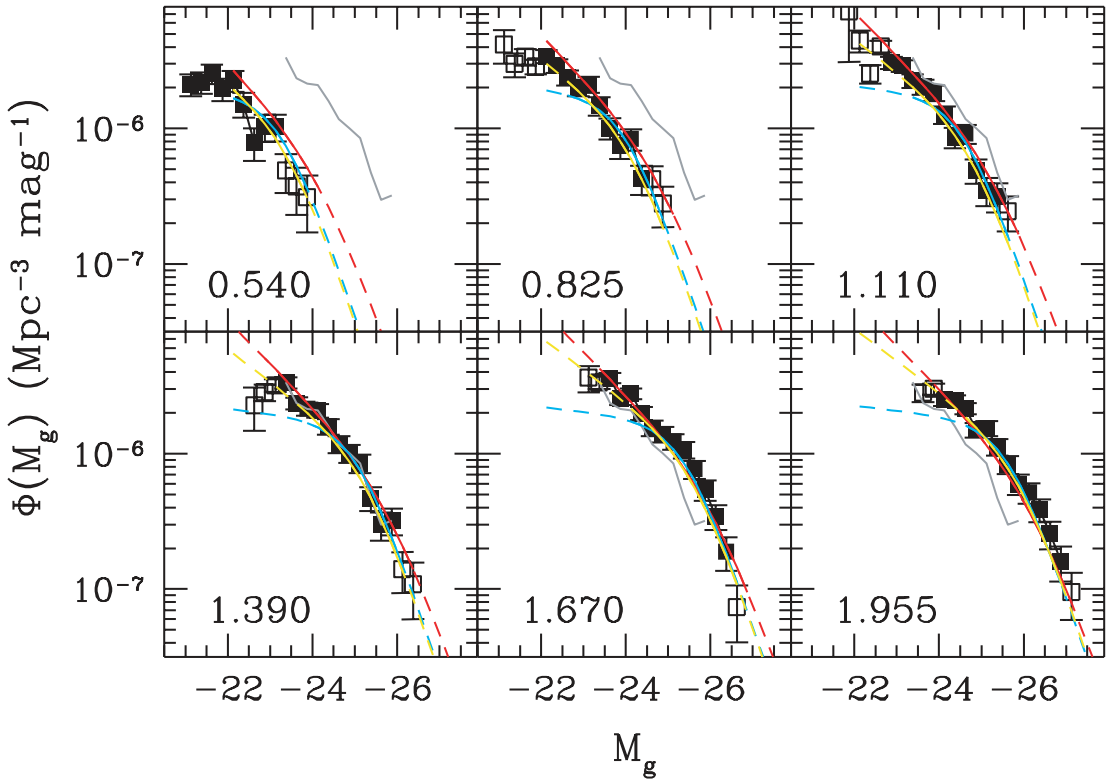

Figure 12. Faint quasar luminosity function for 2SLAQ quasars. Redshift bins are the same as for Croom et al. (2004). Open points are incomplete bins (see Fig. 8). Corrections for photometric, coverage and spectroscopic incompleteness have been applied. Only the quasars within the 41 new plate centres with $0.4 < z < 2.1$ are included. The $z = 1.39$ data are repeated as grey curves in each panel for comparison. Best-fitting models (luminosity evolution characterized by a second-order polynomial in redshift) are shown from Boyle et al. (2000, yellow), Croom et al. (2004, cyan) and this work (red) as solid and dashed lines. The dashed parts of the best-fitting lines indicate where the fits have been extrapolated beyond the data. The faint quasar data suggest a steeper slope than the Croom et al. (2004) models.

Table 3. Summary of maximum-likelihood fits for the parametrization adopted for the 2QZ analysis (double power law with luminosity evolution parametrized as a second-order polynomial in redshift) and our adopted cosmology (Section 1). The redshift limits are $0.4 < z < 2.1$, and objects must be brighter than $M < -22.5$. Here N_Q indicates the number of quasars per square degree expected for $18.0 < g < 21.65$.

Sample	α	β	M^*	k_1	k_2	Φ^*	N_Q	χ^2	ν	P_{χ^2}
Boyle et al. (2000)	−3.41	−1.58	−21.92	1.36	−0.27	9.88e−7	66.8			
Croom et al. (2004)	−3.31	−1.09	−21.61	1.39	−0.29	1.67e−6	54.4			
2SLAQ + Croom et al. (2004)	−3.31	−1.45	−21.61	1.39	−0.29	1.83e−6	83.8	161.5	55	2.1e−12
2SLAQ only	−3.28	−1.78	−22.68	1.37	−0.32	5.96e−7	79.8	149.0	51	1.5e−11

in the last row of Table 3 and the fit is given by the red line in Fig. 12. Owing to the large incompleteness in our last magnitude bin, we have performed these fits to a limiting magnitude of $g < 21.65$ rather than $g < 21.85$. The errors on the parameters are $\sigma_\alpha = 0.2$, $\sigma_\beta = 0.03$, $\sigma_{M^*} = 0.09$, $\sigma_{k_1} = 0.02$ and σ_{k_2}=0.01.

Since there are relatively few bright quasars in our sample to tie down the bright-end slope, we have also attempted to fix all of the parameters except for the faint-end slope (β) and the normalization to those found by Croom et al. (2004), specifically $\alpha = -3.31$, $M^*_g = -21.61 + 5\log h_{70}$, $k_1 = 1.39$ and $k_2 = -0.29$. The resulting faint-end slope is then $\beta = -1.45 \pm 0.03$ (with $\Phi^* = 1.83 \times 10^{-6}\, h^3_{70}$ Mpc^{-3} mag^{-1}). For both of these fits, a χ^2 comparison of this model to the $1/V_a$ data is formally rejected; see Table 3. We also note that there is apparently substantial covariance between the parameters. For example, there is a significant difference in the faint-end slopes of the Boyle et al. (2000) and Croom et al. (2004) analyses (as shown by the cyan and yellow lines in Fig. 12), yet there is only a 1 per cent difference in the total expected counts to the limiting magnitude of the 2QZ survey ($b_J = 20.85$). To the fainter limit of our survey, we find that the final 2QZ parametrization (Croom et al. 2004) significantly underpredicts (by 32 per cent) the total number of quasars to $g < 21.65$, while the Boyle et al. (2000) parameters yield a much better fit to the 2SLAQ data (see Fig. 12 and Table 3). The deviation from the best-fitting 2QZ model can be seen better in the left-hand panel of Fig. 13, where we have normalized our derived values by the best-fitting polynomial evolution model from Croom et al. (2004). The right-hand panel is similar except that the data have all been normalized to our $z = 1.39$ model in order to show the redshift evolution of the quasars better. All of the above suggests that the adopted parametrization is not the optimal one; however, it still has considerable utility in terms of predicting counts of faint quasars and as an input for theoretical models.

We have also attempted to use the parametrizations of the luminosity function that were used by Wolf et al. (2003), since our data,

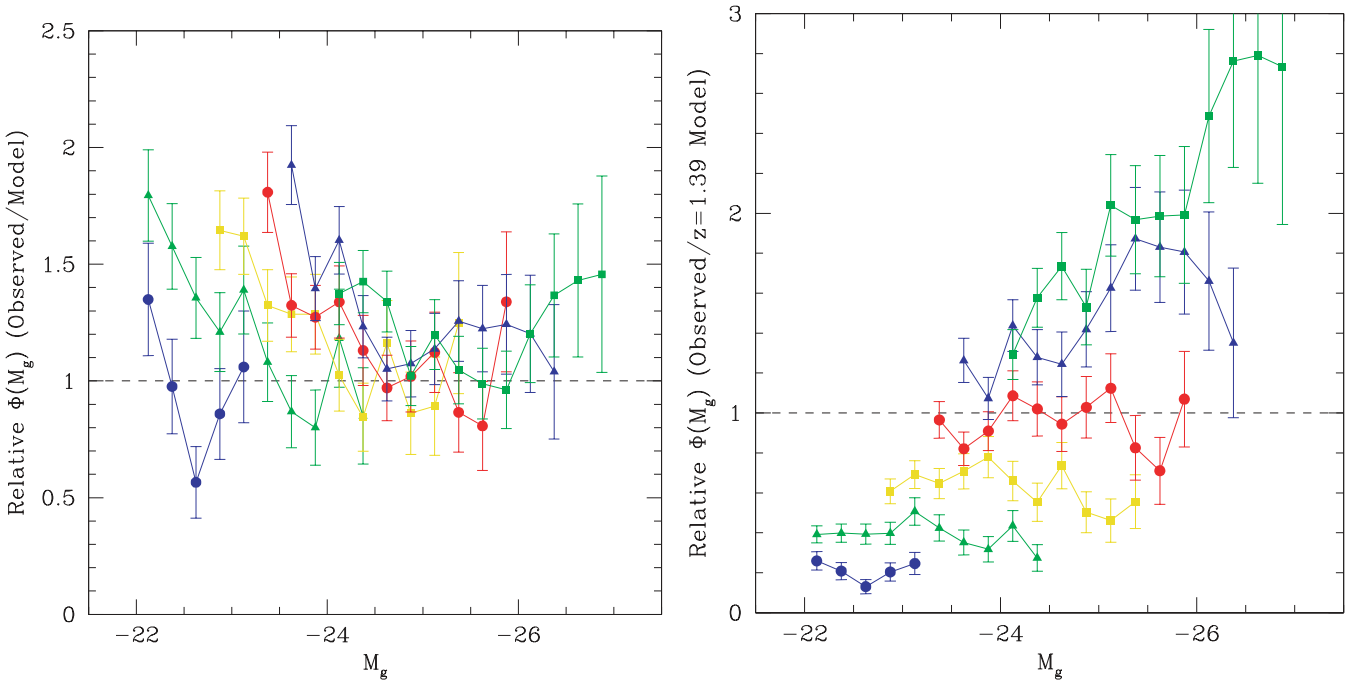

Figure 13. Left: ratio of luminosity function from Fig. 12 to the polynomial evolution models from Croom et al. (2004). Colours and points are as in fig. 20 of Croom et al. (2004), specifically blue circles, green triangles, yellow squares, red circles, blue triangles and green squares, corresponding to redshifts 0.54, 0.825, 1.11, 1.39, 1.67 and 1.955, respectively. Note the deviation from unity at the faint end in each redshift bin. Right: the ratio of the luminosity function to our $z = 1.39$ maximum-likelihood model.

like the data of COMBO-17, appear to show less of a break in the luminosity function than previous work. The best-fitting forms and parameters from Wolf et al. (2003) match the 2SLAQ data over a limited range in redshift and absolute magnitude, but these fits do not agree with the 2SLAQ data at the bright end and for lower redshifts. We were also unable to derive better fits to the 2SLAQ data using such parametrizations, probably because of the lack of dynamic range at the bright end of the distribution. However, it is clear that other parametrizations, like those adopted by COMBO-17, are worth pursuing.

5.4 X-ray comparison

We can test the robustness of the faint end of the 2SLAQ luminosity function by comparing to quasar luminosity functions derived from X-ray-selected samples, which are thought to suffer less incompleteness as a result of the dust-penetrating nature of X-ray photons. In Fig. 14 we compare the $z = 0.825$ and 1.67 redshift bins from Fig. 12 to Croom et al. (2004) and two quasar luminosity functions derived from hard X-ray surveys (Ueda et al. 2003; Barger et al. 2005).

In these comparisons, we have converted between M_g and $\log L$(2–10 keV) as follows. First we take our k-corrected M_g and convert it to (rest-frame) $\log L_g$ (erg s^{-1} cm^{-2} Hz^{-1}) as prescribed by the definition of an AB (Oke & Gunn 1983) magnitude and an absolute magnitude (with an assumed distance of 10 pc):

$$\log L_g = -0.4(M_g - 5 + 48.6) + \log(4\pi) + 2\log(3.086 \times 10^{18}). \quad (8)$$

Next we assume a power-law spectral index of $\alpha_\nu = -0.5$ to convert from rest-frame g (4669 Å) to rest-frame 2500 Å according to

$$\log L_{2500} = \log L_g - 0.5\log(4669/2500). \quad (9)$$

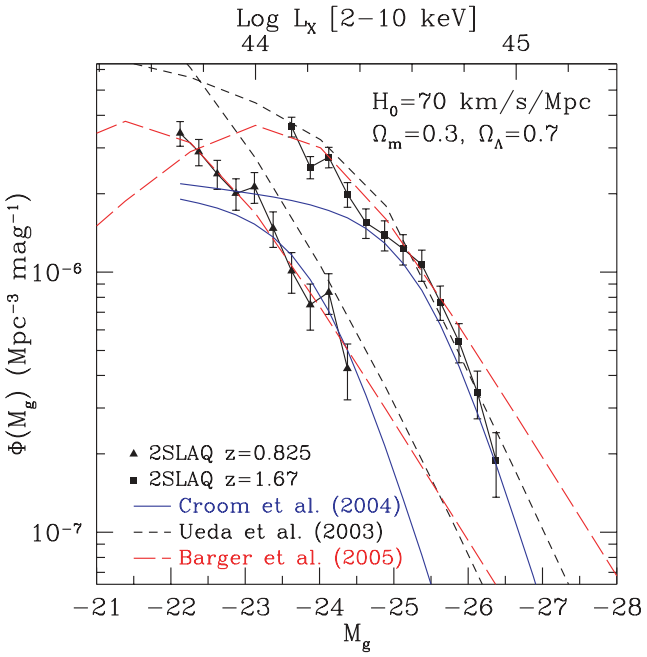

Figure 14. Comparison of the 2SLAQ optical quasar luminosity function with X-ray quasar luminosity functions from the literature. Shown are the $z = 0.825$ (triangles) and $z = 1.67$ (squares) QLF from 2SLAQ and the best-fitting models for those redshifts from three other papers. The models are from Croom et al. (2004, blue solid line), Ueda et al. (2003, dashed black line) and Barger et al. (2005, red long dashed line).

We then extrapolate to $\log L_{2\,\mathrm{keV}}$ assuming a luminosity-dependent 2500 Å to 2 keV slope, α_{ox}, (Vignali, Brandt & Schneider 2003):

$$\alpha_{\mathrm{ox}} = -0.11\log L_{2500} + 1.85 \quad (10)$$

and

$$\log L_{2\,\mathrm{keV}} = \log L_{2500} + \alpha_{\mathrm{ox}} \log \left(\frac{\nu_{2\,\mathrm{keV}}}{\nu_{2500}} \right). \quad (11)$$

[Using the revised α_{ox}–L_{2500} relationship from Strateva et al. (2005) yields somewhat fainter X-ray luminosities ($\sim$0.15 dex) at the bright end of our sample and would slightly flatten the X-ray QLFs in Fig. 14.] Finally, we compute a 2–10 keV luminosity by integrating over the 2–10 keV range assuming a photon index of $\Gamma = 1.9$ ($\alpha_{\mathrm{x}} = -0.9$). For comparison with Ueda et al. (2003) we further correct for the fraction of X-ray Type II active galactic nuclei (AGN) according to their fig. 8 and an optical Type II fraction of 0.5, which is roughly consistent with their fig. 9. In our comparison with the broad-line AGN luminosity function of Barger et al. (2005), we have treated their parametrization as if it were for a 2–10 keV luminosity rather than a 2–8 keV luminosity (since we are primarily concerned with the comparisons of the QLF slope), and we have applied a correction factor of 0.5 in the overall normalization. Furthermore, our comparison with Barger et al. (2005) differs somewhat from their comparison with Croom et al. (2004) in that Barger et al. converted the optical and X-ray luminosities to bolometric luminosities in a manner that assumes a constant α_{ox}, whereas we assumed the luminosity-dependent α_{ox} given above. For both comparisons with X-ray QLFs we have converted the parametrizations to the cosmology adopted herein.

For the sake of facilitating the comparison of optical QLFs to X-ray QLFs, we note that, in the syntax used by Ueda et al. (2003) in their equation (6) [and similar notation used by Barger et al. (2005) in their equation (1)], $\phi_M = A/2.5, \alpha = -(\gamma_1 + 1)$ and $\beta = -(\gamma_2 + 1)$, where ϕ_M, α and β are defined as in (Peterson 1997, equation 11.33) (and similarly by Croom et al. 2004, equation 11).

In each case, the X-ray luminosity functions show less curvature in the faintest 2SLAQ bins than does the best-fitting model from 2QZ. This comparison is not meant to be strictly quantitative since X-ray-selected samples are more sensitive to obscured quasars and the conversion between M_B and L_{X} involves a number of tenuous assumptions. However, these comparisons confirm that the steeper 2SLAQ faint-end slope, while based on large correction factors, is quite reasonable. In particular, the agreement with the results of Barger et al. (2005) is remarkable.

6 DISCUSSION AND CONCLUSIONS

We have compiled a sample of 5645 quasars with $18.0 < g < 21.85$ and $z < 3$ using imaging data from the SDSS and the spectra from the 2dF facility at the AAT. We find a clear turnover in the optical number counts; a single power law is not a good fit over the magnitude range sampled. For $20 < g < 20.6$, the 2SLAQ number counts show a slight (but statistically insignificant) excess over previous surveys, but the cumulative number counts are roughly consistent with the faintest surveys to 22nd magnitude.

In terms of the luminosity function, we find good agreement with the 2QZ results from Croom et al. (2004) at the bright end, but the faint-end 2SLAQ data require a steeper slope (higher density of quasars) than the 2QZ results from Croom et al. The previous 2QZ results from Boyle et al. (2000) agree significantly better with 2SLAQ at the faint end. The lack of a well-defined characteristic luminosity and covariance between the maximum-likelihood parameters can explain the good bright-end agreement between the parametrizations studied and the faint-end disagreement between 2SLAQ and the final 2QZ results Croom et al. (2004). Comparing to Type I quasar luminosity functions derived from X-ray samples suggests that the slope of the faint end of the 2SLAQ QLF is more accurate than the extrapolated faint-end slope of Croom et al. (2004).

An understanding of the quasar luminosity function is an important ingredient for many different types of extragalactic investigations. In particular, as has been stressed by those working with X-ray-selected samples, investigations that depend on the optical QLF explicitly may need to be reconsidered as a result of recent revisions in the luminosity function of unobscured AGNs (not to mention obscured AGNs). Many investigations have an explicit dependence on the optical QLF: for example, Bianchi, Cristiani & Kim (2001) in their analysis of the ultraviolet background; Hamilton, Casertano & Turnshek (2002) in their estimate of the quasar host-galaxy luminosity function; Yu & Tremaine (2002) in their investigation of the growth of black holes; Croom et al. (2002) and Wake et al. (2004) regarding the clustering of AGN; Oguri (2003) in his determination of the expected number of lensed quasars; Richards et al. (2004b) in their assessment of the lensing probability of the most luminous high-redshift quasars; and Fan et al. (2001b) in terms of the evolution of quasars from $z = 0$ to 6. The QLF has taken on even greater importance in recent years with the realization that most massive galaxies host supermassive black holes, the correlation between black hole mass and stellar velocity dispersion (e.g. Magorrian et al. 1998; Ferrarese & Merritt 2000; Gebhardt et al. 2000), and the possibility that feedback from quasars may play a role in the evolution of galaxies in general (e.g. Begelman 2004). In particular, models like those of Kauffmann & Haehnelt (2000), Wyithe & Loeb (2002) and others that attempt to explain the evolution of galaxies and quasars rely on comparison with accurate observational determinations of the QLF.

In fact, although the optical QLF presented herein is arguably the most robust determination to date for a large optically selected sample, for many applications an X-ray or far-infrared QLF is more appropriate. That said, the luminosity function of optically selected quasars will remain an important tool for extragalactic astronomy. The primary reason for this is the sheer size of the optical quasar sample (likely over 300 000 in the current SDSS imaging data alone; Richards et al. 2004a). While the deepest X-ray surveys may uncover thousands of AGNs per square degree, they do so over only a fraction of a square degree and the sum total area of the sky covered by both *Chandra* and *XMM–Newton* is unlikely ever to exceed even 1 per cent. Infrared surveys with *Spitzer* will cover a somewhat larger area than X-ray surveys, but not at nearly the same space density as in the X-ray or with nearly the same total number as in the shallower, but much wider, optical surveys. Thus, this sample of faint quasars and the luminosity function derived from it will continue to provide important inputs to future extragalactic investigations such as the Dark Energy Survey (DES) and the Large Synoptic Survey Telescope (LSST).

ACKNOWLEDGMENTS

Funding for the creation and distribution of the SDSS Archive has been provided by the Alfred P. Sloan Foundation, the Participating Institutions, the National Aeronautics and Space Administration, the National Science Foundation, the US Department of Energy, the Japanese Monbukagakusho and the Max Planck Society. The SDSS website is http://www.sdss.org/. The SDSS is managed by the Astrophysical Research Consortium (ARC) for the Participating Institutions. The Participating Institutions are the University of Chicago, Fermilab, the Institute for Advanced Study, the Japan Participation Group, the Johns Hopkins University, the Korean Scientist Group, Los Alamos National Laboratory, the Max-Planck-Institute

for Astronomy (MPIA), the Max-Planck-Institute for Astrophysics (MPA), New Mexico State University, University of Pittsburgh, University of Portsmouth, Princeton University, the United States Naval Observatory and the University of Washington. Spectroscopic observations were performed with the 2dF instrument on the Anglo-Australian Telescope, and we thank the staff of the Anglo-Australian Observatory for their support. We thank Michael Weinstein and Michael J. I. Brown for assistance with code development. DPS and DEVB were supported in part by NSF grant AST-0307582. MAS was supported in part by NSF grant AST-0307409.

REFERENCES

Abazajian K. et al., 2003, AJ, 126, 2081
Avni Y., Bahcall J. N., 1980, ApJ, 235, 694
Bailey J. et al. 2003, http://www.aao.gov.au/2df/manual.html
Barger A. J., Cowie L. L., Mushotzky R. F., Yang Y., Wang W.-H., Steffen A. T., Capak P., 2005, AJ, 129, 578
Begelman M. C., 2004, in Ho L. C., ed., Carnegie Observatories Astrophysics Ser. Vol. 1, Coevolution of Black Holes and Galaxies. Cambridge Univ. Press, Cambridge, p. 375
Bianchi S., Cristiani S., Kim T.-S., 2001, A&A, 376, 1
Blanton M. R., Lin H., Lupton R. H., Maley F. M., Young N., Zehavi I., Loveday J., 2003, AJ, 125, 2276
Boyle B. J., Fong R., Shanks T., Peterson B. A., 1987, MNRAS, 227, 717
Boyle B. J., Shanks T., Peterson B. A., 1988, MNRAS, 235, 935
Boyle B. J., Fong R., Shanks T., Peterson B. A., 1990, MNRAS, 243, 1
Boyle B. J., Jones L. R., Shanks T., 1991, MNRAS, 251, 482
Boyle B. J., Shanks T., Croom S. M., Smith R. J., Miller L., Loaring N., Heymans C., 2000, MNRAS, 317, 1014
Cannon R. D. et al., 2003, AAO Newslett., 103, 8
Croom S. M., Smith R. J., Boyle B. J., Shanks T., Loaring N. S., Miller L., Lewis I. J., 2001, MNRAS, 322, L29
Croom S. M., Boyle B. J., Loaring N. S., Miller L., Outram P. J., Shanks T., Smith R. J., 2002, MNRAS, 335, 459
Croom S. M., Smith R. J., Boyle B. J., Shanks T., Miller L., Outram P. J., Loaring N. S., 2004, MNRAS, 349, 1397
Fan X., 1999, AJ, 117, 2528
Fan X. et al., 2001a, AJ, 121, 54
Fan X. et al., 2001b, AJ, 122, 2833
Ferrarese L., Merritt D., 2000, ApJ, 539, L9
Fukugita M., Ichikawa T., Gunn J. E., Doi M., Shimasaku K., Schneider D. P., 1996, AJ, 111, 1748
Gebhardt K. et al., 2000, ApJ, 539, L13
Gunn J. E. et al., 1998, AJ, 116, 3040
Hamilton T. S., Casertano S., Turnshek D. A., 2002, ApJ, 576, 61
Hawkins M. R. S., Veron P., 1995, MNRAS, 275, 1102
Hewett P. C., Foltz C. B., Chaffee F. H., 1993, ApJ, 406, L43
Hogg D. W., 1999, preprint (astro-ph/9905116)
Hogg D. W., Finkbeiner D. P., Schlegel D. J., Gunn J. E., 2001, AJ, 122, 2129
Ivezić Ž. et al., 2002, AJ, 124, 2364
Kauffmann G., Haehnelt M., 2000, MNRAS, 311, 576
Kennefick J. D., Djorgovski S. G., de Carvalho R. R., 1995, AJ, 110, 2553
Koo D. C., Kron R. G., 1988, ApJ, 325, 92
Lewis I. J. et al., 2002, MNRAS, 333, 279
Lupton R. H., Gunn J. E., Szalay A. S., 1999, AJ, 118, 1406
Lupton R. H., Gunn J. E., Ivezić Z., Knapp G. R., Kent S., Yasuda N., 2001, in Harnden F.R. Jr., Primini F.A. and Payne H.E., eds, ASP Conf. Ser. Vol. 238, Astronomical Data Analysis Software and Systems X. Astron. Soc. Pac., San Francisco, p. 269
Magorrian J. et al., 1998, AJ, 115, 2285
Marano B., Zamorani G., Zitelli V., 1988, MNRAS, 232, 111
Oguri M., 2003, MNRAS, 339, L23
Oke J. B., Gunn J. E., 1983, ApJ, 266, 713
Padmanabhan N. et al., 2005, MNRAS, 359, 237
Page M. J., Carrera F. J., 2000, MNRAS, 311, 433
Peterson B. M., 1997, An Introduction to Active Galactic Nuclei. Cambridge Univ. Press, Cambridge
Pier J. R., Munn J. A., Hindsley R. B., Hennessy G. S., Kent S. M., Lupton R. H., Ivezić Ž., 2003, AJ, 125, 1559
Press W. H., Teukolsky S. A., Vetterling W. T., Flannery B. P., 1992, Numerical Recipes in C. The Art of Scientific Computing, 2nd edn. Cambridge Univ. Press, Cambridge
Richards G. T. et al., 2001, AJ, 121, 2308
Richards G. T. et al., 2002, AJ, 123, 2945
Richards G. T. et al., 2004a, ApJS, 155, 257
Richards G. T. et al., 2004b, AJ, 127, 1305
Schlegel D. J., Finkbeiner D. P., Davis M., 1998, ApJ, 500, 525
Schmidt M., 1968, ApJ, 151, 393
Schmidt M., Green R. F., 1983, ApJ, 269, 352
Schmidt M., Schneider D. P., Gunn J. E., 1995, AJ, 110, 68
Schneider D. P. et al., 2003, AJ, 126, 2579
Schneider D. P. et al. 2005, AJ, in press
Scranton R. et al., 2002, ApJ, 579, 48
Smith J. A. et al., 2002, AJ, 123, 2121
Spergel D. N. et al., 2003, ApJS, 148, 175
Stoughton C. et al., 2002, AJ, 123, 485
Strateva I., Brandt N., Schneider D., Vanden Berk D., Vignali C., 2005, AJ, in press (astro-ph/0503009)
Telfer R. C., Zheng W., Kriss G. A., Davidsen A. F., 2002, ApJ, 565, 773
Ueda Y., Akiyama M., Ohta K., Miyaji T., 2003, ApJ, 598, 886
Vanden Berk D. E. et al., 2001, AJ, 122, 549
Vanden Berk D. E. et al., 2005, AJ, 129, 2047
Vignali C., Brandt W. N., Schneider D. P., 2003, AJ, 125, 433
Wake D. A. et al., 2004, ApJ, 610, L85
Warren S. J., Hewett P. C., Osmer P. S., 1994, ApJ, 421, 412
Weinstein M. A. et al., 2004, ApJS, 155, 243
Wolf C., Wisotzki L., Borch A., Dye S., Kleinheinrich M., Meisenheimer K., 2003, A&A, 408, 499
Wyithe J. S. B., Loeb A., 2002, ApJ, 581, 886
York D. G. et al., 2000, AJ, 120, 1579
Yu Q., Tremaine S., 2002, MNRAS, 335, 965
Zitelli V., Mignoli M., Zamorani G., Marano B., Boyle B. J., 1992, MNRAS, 256, 349

This paper has been typeset from a TEX/LATEX file prepared by the author.